Antarctic Coastline Detection using Snakes[1]

Tobias Klinger, Marcel Ziems, Christian Heipke, Hannover; Hans Werner Schenke, Norbert Ott, Bremerhaven

Summary: In this paper we present an approach for automatic coastline detection from images based on snakes (parametric active contours) and apply it to Landsat images from Antarctica. Snakes require the definition of an energy functional that reflects the underlying coastline model. For Antarctica the coastline appearance in the images is heterogeneous. Therefore, it is not possible to use a single model only. After inspecting the images to be used we formulate three different transition models that match a large part of the Antarctic coastline: (a) from ice shelf to water, (b) from ice shelf to sea ice and (c) from rocky terrain to water. For each of the three models the energy terms are optimised based on the radiometric properties of the adjacent regions as well as the curvature and the potential change-rate of the coastline itself. A supervised classification for the three classes *ice*, *water* and *rocky terrain* controls the whole process by selecting the most applicable model for a given image region along the coastline. We present results for the extraction of approximately 12% of the Antarctic coastline from an up-to-date Landsat mosaic.

Zusammenfassung: *Küstenliniendetektion in der Antarktis mit Hilfe von Snakes.* In diesem Artikel präsentieren wir einen Ansatz zur automatischen Erfassung von Küstenlinien mit Hilfe von Snakes (parametrische aktive Konturen) und verwenden diesen für die Detektion der Antarktischen Küstenlinie in Landsat Bildern. Snakes erfordern die Definition eines Energiefunktionals, welches das zugrundeliegende Küstenlinienmodell beschreibt. In der Antarktis ist die Erscheinung der Küstenlinie in optischen Bildern inhomogen. Daher ist es nicht hinreichend, mit einem einzelnen Modell zu arbeiten. Wir formulieren drei verschiedene Übergangsmodelle, die einen großen Teil der Antarktisküste abdecken: (a) von Schelfeis zu Wasser, (b) von Schelfeis zu Meereis und (c) von felsigem Gelände zu Wasser. Für jedes dieser Modelle optimieren wir die Energieterme auf Grundlage der speziellen radiometrischen Eigenschaften im Bereich der Küstenlinie sowie deren jeweils zu erwartender Kurvigkeit und Veränderungsrate. Eine überwachte Klassifizierung dieser Regionen für die Klassen *Eis*, *Wasser* und *Felsen* kontrolliert den Prozess. Wir zeigen Ergebnisse der Extraktion aus einem aktuellen Landsat-Mosaik für circa 12% der Antarktischen Küstenlinie.

1 Introduction

Mapping a coastline is a comprehensive task, traditionally carried out by manual digitization from images. Exploiting remotely sensed imagery by means of automatic image-processing techniques is an increasingly important approach, especially where the need for frequently updated coastline data is high. Considering the coastline in a temporal sense, the update cycle of the coastline data is limited by the revisit time of the imaging sensor, and the accuracy of the coastline is influenced by the ground sampling distance of the images. The availability of space borne imagery has increased in recent decades due to a larger number of related satellites, including Radarsat-1, Landsat ETM+ or MODIS on board Aqua/Terra.

In Antarctica, the coastline attains particular attention, as it constitutes the border of the vast ice sheet, influencing our climate and significantly contributing to sea level rise when melting (Houghton et al. (eds.) 2001). The mass balance of the Antarctic ice sheet changes due to surface and basal melting related to climate change, resulting in many floating ice shelves around the periphery of the continent.

---

[1] Extended version of a paper published in The International Archives of the Photogrammetry, Remote Sensing and Spatial Information Sciences, Vol. XXXVIII, Part 4, 2010, 7 S., (on CD-ROM) .

The link between the break-up of ice shelves and climatic effects such as global warming and sea level rise is discussed e.g. in (BINDSCHADLER 1998, SCAMBOS et al. 2000). In order to quantify such effects accurate and up-to-date coastline information is necessary.

During the last 15 years, imagery of three high/medium resolution satellites has been used to create image mosaics of the Antarctic continent. Two SAR image mosaics have been generated from Radarsat-1 data in 1997 and 2000, i.e. the Radarsat Antarctic Mapping Mission 1 (AMM-1) and its modified counterpart (MAMM-2) (JEZEK et al. 2002). The MODIS Mosaic of Antarctica (MOA) has been derived from images of the MODIS sensors acquired from 2003-2004 (SCAMBOS et al. 2007). A Landsat Image Mosaic of Antarctica (LIMA) with a ground sample distance of 240 m, with images taken from 1999 to 2003, has been released in support of the International Polar Year in 2007/2008 (BINDSCHADLER et al. 2008). Due to orbit inclination, LIMA covers Antarctica only from 82.5° southern latitude northwards. Two coastlines have been extracted from the Radarsat Antarctic Mapping Project (RAMP) mosaic in a semiautomatic way and another one from MOA completely manually. To our knowledge, no complete coastline has been extracted yet on the basis of LIMA.

With respect to the fractal nature of coastlines (MANDELBROT 1967), the length of the Antarctic coastline as detected in modern high resolution satellite imagery reaches the size of the Earth's equator (cmp. LIU & JEZEK 2004), thus frequently mapping the coastline is a formidable task. As mentioned before, visual interpretation of the imagery is still often being applied in modern mapping projects (e.g. SCAMBOS et al. 2007). This process yields a seamless and unique realization of the coastline, but suffers from the immense time consumption and the subjectivity of the observer. In the spirit of map updating we consider the existing coastline as an additional input when automatically creating an up-to-date version. Fig. 1 visualizes our idea of taking advantage of a given coastline for detecting the up-to-date position. We employ snakes (active contours) introduced by KASS et al. (1988), with the extended external force field by XU & PRINCE (1997), referred to as Gradient Vector Flow (GVF) snakes.
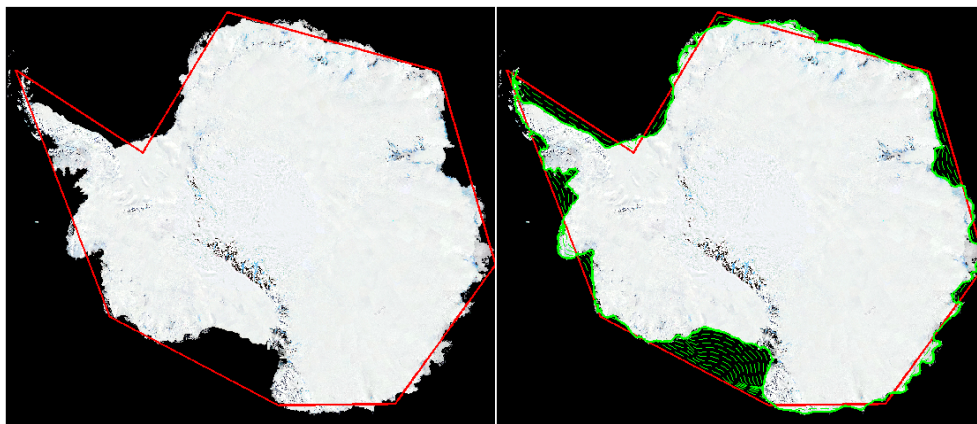
Fig. 1: Coastline detection for the Antarctic context. Initialisation of the snake with a polygon of eight supporting points connected by the red line (left); result of the coastline detection using snakes: the result is shown as a green line and every 10th iteration is symbolized by a green dotted line (right).

The remainder of the paper is structured as follows. In the next chapter we discuss related approaches that deal with coastline detection in digital imagery. Chapter 3 specifies our model definition for the different types of coastlines we deal with. In chapter 4 we describe the incorporation of these different model types into our snake algorithm. Chapter 5 contains some results of our approach including a quantitative evaluation of completeness, correctness and geometric accuracy. We conclude the paper in chapter 6.

2 Related Work

In the following, we give an overview of approaches that have been proposed towards automated coastline extraction in remotely sensed images. Basically, the methods can be divided into region-based classification techniques and methods based on edge detection.

RYAN et al. (1991) applied texture classification to scanned aerial photographs based on a neural network. The coastline is defined as the boundary between different homogeneous regions. Templates for the calculation of the neighbourhood information of the selected texture features lead to smoothed results but reduce the geometric accuracy. MUSLIM et al. (2006) utilize soft classification methods in coarse resolution images for predicting the proportion of land and water coverage in a super-resolution mapping step. Soft classification yields sub-pixel accuracy, but may fail for land-cover classes excluded from the training sites. LIU & JEZEK (2004) classify regions adjacent to the Antarctic coastline based on grey values of Radarsat-1 images, which usually provide better contrast for the Antarctic context than available optical sensors. The classification strategy exploits the bimodal character of the SAR image histogram in coastal regions. Locally adaptive contrast ratio thresholds are determined to separate image regions. After the classification step several shape descriptors are employed to generate plausible regions, whose boundaries are the basis for coastline extraction. The practical applicability of the approach was proven when the complete Antarctic coastline was extracted from a SAR image mosaic of 25 m and 100 m resolution with a relative precision of approximately one pixel.

Methods based on automatic edge detection have been applied to detect coastlines in remotely sensed images, but to the best of our knowledge not yet for the Antarctic context. MASON & DAVENPORT (1996) presented a hierarchical strategy that combines a region-based classification and an edge-based strategy. In a first step a SAR image of reduced resolution is used to detect an approximate position of the coastline by classification of the adjacent regions. Subsequently, an active contour model (KASS et al. 1988) is applied to find a geometrically accurate solution in the image of original resolution. A further development of this idea is described in DELLA ROCCA et al. (2004) where the initial contour is derived from the output of a wavelet operation. NIEDERMEIER et al. (2000) detect edges in SAR images by segmenting the image into land, water and coastal areas using a block tracing algorithm. The vectorized water-coastal region boundary of the blocktracing is utilized as initialisation of a snake algorithm.

Region based techniques for coastline detection in Antarctica using optical imagery is stated to be less appropriate due to lower contrast than in SAR imagery. In fact, it remains difficult to separate regions like annual sea ice and ice shelf by classification because of their spectral similarity. Therefore, none of the region based methods can be expected to handle the occurrence of the ice-to-ice constellation as frequently observed in Antarctica with optical images as input. It was also found that using global statistics for training may provide an inappropriate description of the classes to be distinguished locally and hence decrease the accuracy of coastline prediction (MUSLIM et al. 2006). When using the traditional snake approach, the initialisation must be very close to the salient feature for obtaining the correct result. Furthermore, without local adaptation the snakes would fail in the Antarctic context, since the coastline appearance varies broadly from one area to the next.

3 Model Definition

The spectral and geometric characteristics of the Antarctic coastline in optical imagery are heterogeneous, so that no single coastline model can adequately reflect the different appearance. On the basis of the Landsat mosaic LIMA we therefore formulate three different models that match a large part of the Antarctic coastline, i.e. the transition from ice shelf to water, from ice shelf to sea ice and from rocky terrain to water (Fig. 2), where "ice shelf" includes grounded as well as floating ice shelf, and "sea ice" is not older than one year, and is frequently covered by snow, which makes it hard to distinguish from ice shelf. The fourth model in this row would be the transition from rocky terrain to sea ice. This model, however, is not regarded further, since it appears only very seldom. The following characteristics are considered with regard to the definition of the snake energy terms (see also chapter 4).

3.1 *Ice Shelf to Water*

The transition from ice shelf to water is expected to always show a clear contrast due to the much lower albedo of water than the one of snow or ice. The adjacent regions are mostly homogeneous, except for the existence of floes preloaded to the offshore side. Hence, for this model a high edge response in the image indicates the location of the coastline. Except for rifts, the shape of the coastline is mostly smooth. Floating and calving ice shelves can cause planimetric movements of the coastline of up to 1 km per year (BRUNT et al. 2010).


Fig. 2: LIMA subsets with instances of the transitions from ice shelf to water (left); ice shelf to sea ice (centre; the coastline extends from bottom left to the upper right corner as pointed out by the red arrows); and rocky terrain to water (right).

3.2 *Ice Shelf to Sea Ice*

The transition from ice shelf to sea ice exhibits little contrast in intensity, colour and texture (see Fig. 2, centre). Sharp changes of slope perpendicular to the coastline direction often causes the thick ice shelf fronts to cast shadows on the sea ice or to appear very bright, especially at low sun angles. In the image these effects result in a thin line that usually does not exceed a width of one pixel. Shadows cause the coastline to appear as a dark line while the illumination at low sun angles results in a bright line. The coastline is mostly smooth and undergoes the same geometric changes over time as the *ice shelf to water* coastline.

3.3 *Rocky Terrain to Water*

The transition from rocky terrain to water is difficult to recognise in the image (see Fig. 2, right), while the contrast between rock and ice further inbound the continent, which often occurs in the vicinity of rocks, is rather high. Nevertheless, there is a noticable difference in terms of colours between the rocks and the water, which results in characteristic differences in the HSI (hue, saturation, intensity) space (see Fig. 3). The coastline is not expected to significantly change its geometric position over time. In contrast to the previously discussed models, the coastline is rather curvy due to rifts and bays.
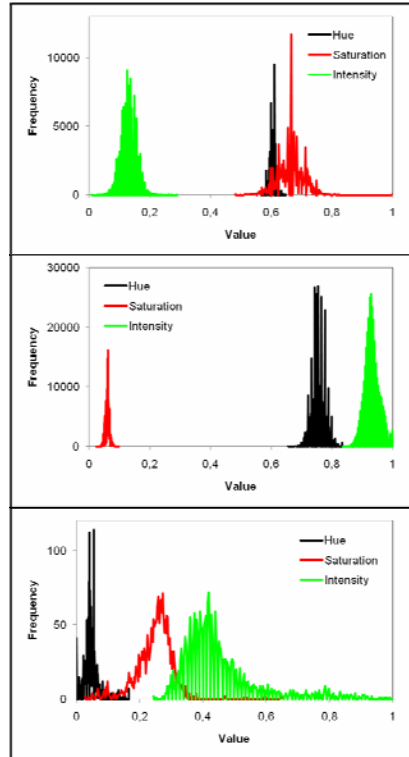
Fig. 3: Histograms of normalised hue, saturation and intensity values for the classes water (top), ice (centre) and rock (bottom).

4 Strategy

We follow MASON & DAVENPORT (1996) and present a method which uses snakes as the core algorithm. It is known that snakes require a sufficiently good initialisation to yield an accurate and reliable solution. In our approach the initialisation is derived from the RAMP coastline, which is represented as a polygon. We define a new coastline model for optical data consisting of three individual and different snake models. For this purpose representative regions on both sides along the initial coastline are classified so that the appropriate snake model can be selected automatically. The related snake algorithm then computes the position of the coastline. By incorporating the Gradient Vector Flow (GVF) into our image energy description, we achieve a higher attraction range for inititalisations further away from the final coastline. In the following the automated selection of the model and the strategy for employing the model within a snake algorithm are described in detail.

4.1 *Pre-processing*

Due to the heterogeneous coastline characteristics as well as the immense data volume it is not reasonable to process the complete Antarctic coastline simultaneously. Instead, the Landsat mosaic is segmented into a number of tiles of equal size (here: 460 tiles of 240² km² each), and snakes are placed over each tile that contains a section of the given coastline. Out of the 460 tiles, only those are considered further, which overlap with the given RAMP coastline.

4.2 *Model Selection*

An automated analysis is carried out for each image tile to find the best-matching model. For this task we subdivide the coastline into line-segments with an equal number of polygon points. This idea seems to be more promising than choosing equally long sections since the distance between the polygon points is smaller where the coastline is more structured leading to more frequent transitions within different object types. The line-segments are classified into one of the three models described in chapter 3 using features from regions on both sides of the line-segment, shifted by a certain offset in off- and onshore direction (see Fig. 4). We set the offset with respect to the largest speed expected for the floating ice shelf (1km per year) and the time interval between the acquisition of the previously and currently used imagery (two years in our case) to be 2 km.

For classification we used a simple nearest neighbour algorithm. We trained the classifier using features from manually selected areas from different tiles of the LIMA mosaic (Note that for mosaic generation the different original images were radiometrically adjusted to each other. Therefore it was possible to select the training areas from different parts of the coastline without problems due to multi-temporal data acqusition etc.). First tests with features from RGB space yielded unsatisfactory results. We therefore used features from HSI space. In this colour space water has a characteristic distribution of saturation values compared to ice and rock (see Fig. 3 and discussion above), whereas ice is significantly brighter than the other classes with regard to the intensity channel and rock appears slightly redish/brownish leading to a low angle of hue. We found the best classificaton results with the following three features: the average region values of saturation and intensity and the percentage of pixels with hue values in the range of $[0;\pi/2]$. The last feature is able to detect rocks also in the presence of ice (see again Fig. 3). The classification results for the corresponding regions on either side of the given coastline are then combined to select the correct snake model. Hence, we consider the coastline types according to the corresponding regions as *ice shelf to water*, *ice shelf to sea ice* or *rocky terrain to water* and select the related snake model for further processing.
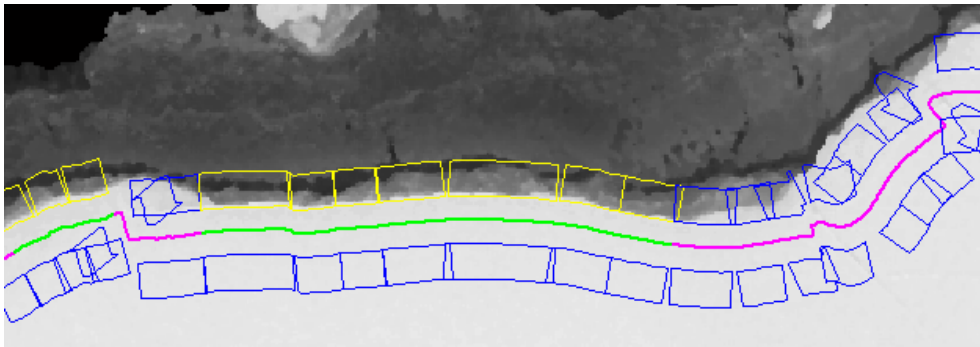
Fig. 4: Classification results: line segments coloured in relation to the classification result, i.e. green for water-ice and magenta for ice-ice boundary. The analysed regions are coloured in accordance with the detected object type: yellow for water and blue for ice.

4.3 *Parameterisation of Snakes*

Snakes require the definition of an energy functional that reflects the underlying coastline model. For each of the three different models the energy terms and related parameters are optimised based on the radiometric properties of the adjacent regions as well as the curvature and the potential change-rate of the considered coastal region. Traditionally, a snake is considered as a curve $\mathbf{v}(s) = (x(s),y(s))$ parameterised with the arc length $s \in [0,1]$, that iteratively moves in the image domain $I(x,y)$ until its energy functional E^*_{Snake} is minimised (KASS et al. 1988):

$$E^*_{snake} = \int E_{int}(\mathbf{v}(s)) + E_{con}(\mathbf{v}(s)) + E_{img}(\mathbf{v}(s))ds \qquad (1)$$

The internal energy E_{int} controls the shape of the snake and thus varies with every deformation of the curve. Typically the bending and stretching of **v** are the considered internal snake characteristics, modelled by the first and second derivatives of **v** with respect to s:

$$E_{int}(\mathbf{v}(s)) = \frac{1}{2} \cdot \left[\alpha \cdot |\mathbf{v}'(s)|^2 + \beta \cdot |\mathbf{v}''(s)|^2 \right]$$

(2)

where E_{int} = internal energy

        v', **v''** = derivations of **v** with respect to s

        α = elasticity parameter

        β = rigidity parameter

The elasticity and rigidity parameters α and β act as weighting factors of the first and second order term of eq. 2. The first term controls the length of the snake. Large values for α stretch the coastline and smooth the effect of local disturbances in the image energy. The second term controls the snake curvature: β allows to adapt the shape properties of the coastline models, e.g. large values for β lead to a straighter coastline while small values allow a high curvature coastline.

The constraint energy E_{con} and the image energy E_{img} of eq. 1 are considered as context dependent external influences that affect the snake's position, being responsible for iterative movements and deformations. E_{con} can make the snake move towards or away from fixed points or lines. In our current implementation constraints are not considered, however, they could be easily added, e.g. for pulling the snake towards manually selected points.

The image energy affects the position of the snake with respect to the features in the image. E_{img} can be considered as a scalar potential energy that is defined for each pixel as a function of the grey value $I(x,y)$ so that it adopts smaller values at salient features. E_{img} can hence be calculated once in advance before starting the iterative optimisation procedure.

Since for the present approach we distinguish different types of coastline, we use different image energy definitions that attract the snake to lines or edges in the image according to the associated model. In the literature, the image energy for lines is often simply the image function itself (KASS et al. 1988), with the sign indicating if the snake is to be attracted to light (-) or dark lines (+). As explained above, for the detection of coastlines that match the line model, the snake must be attracted to both, light and dark lines. For line detection we employ the Steger line operator (STEGER 1998). The image energy for the line model results from a binary decision as

$$E_{img}^{line}(x, y) = \begin{cases} 1, \text{ if } (x, y) \in (L_- \vee L_+) \\ 0 \qquad\qquad\quad otherwise \end{cases}$$

(3)

with L_- being the set of light lines and L_+ the set of dark lines, respectively, detected by the line operator. For edges, the energy term is traditionally defined as the negative squared magnitude of the gradient image. We apply the Canny operator (CANNY 1986) for edge detection yielding image gradients $\nabla(x,y)$ and binarisation with respect to an edge threshold t as

$$E_{img}^{edge}(x, y) = \begin{cases} 1, \text{ if } \quad |\nabla(x, y)| > t \\ \quad 0 \quad otherwise \end{cases}$$

(4)
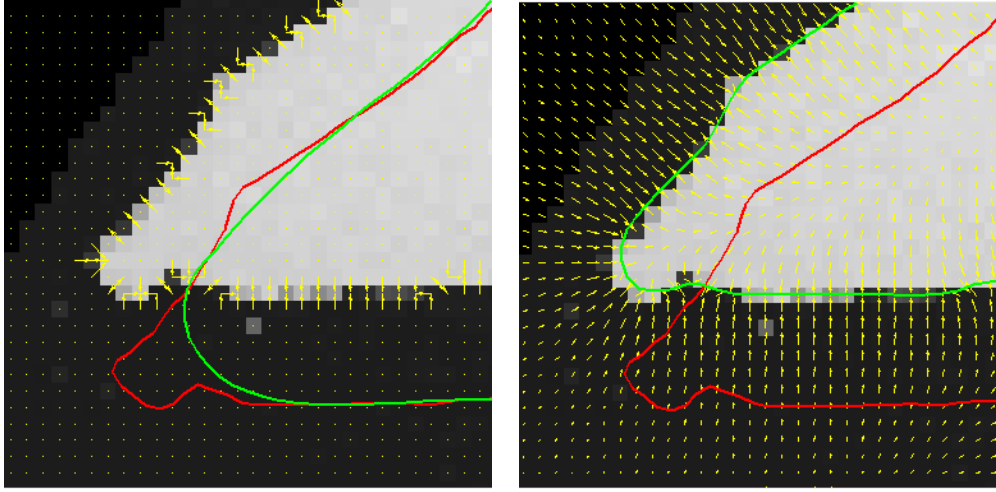
(a)   (b)

Fig. 5: Vector field marked by yellow arrows: a) standard vector field with vectors pointing towards the edges; the snake cannot converge to the correct solution from a poor initialisation (red) yielding a wrong result (green); b) GVF field, where the snake can be initialized anywhere in the GVF field for being pulled towards an edge, thus the result is correct.

The capture range of the traditional image energy is limited with respect to the width of the template of the gradient operator (see Fig. 5a). As soon as the distance to the initialisation is only slightly larger than the capture range of the image energy, convergence is not assured. To overcome this limitation, XU & PRINCE (1997) have extended the energy field by applying a generalised diffusion equation to the response of the image energy term called Gradient Vector Flow (GVF) field. The increased capture range is visualized in Fig. 5b. Moreover, the capture range of the GVF related snake also enables the contour to progress into concave parts of the boundary.

In order to minimise the snake energy E^*_{snake} the related Euler equation (eq. 5) must be solved:

$$\alpha \cdot \mathbf{v}''(s) - \beta \cdot \mathbf{v}'''' - \nabla E_{img} = 0 \qquad (5)$$

which leads to:

$$\mathbf{v}(t) = (\mathbf{A} + \gamma \cdot \mathbf{I})^{-1} \cdot \left[\gamma \cdot \mathbf{v}(t-1) - \kappa \cdot f_{\mathbf{v}}(\mathbf{v}(t-1)) \right] \qquad (6)$$

where $\mathbf{v}(t)$ = snake representation at time t

   $\mathbf{A}$ = design matrix

   γ = step size (viscosity factor)

   $\mathbf{I}$ = identity matrix

   κ = weight factor for external energy

   $f_{\mathbf{v}}$ = gradient values from image energy

In eq. 6 the snake is made dynamic by describing **v** as a function of time. The matrix $\mathbf{A} + \gamma \cdot \mathbf{I}$ is a pentadiagonal banded matrix and γ controls the step size that influences the viscosity of the snake (for details of snake optimisation see KASS et al. (1988), FUA (1995), and BUTENUTH (2008)).

5 Experiments and Results

In this chapter we report the results achieved with the described coastline extraction approach. Until

now, we have processed approximately 5000 km or 12% of the Antarctic coastline around the Weddell Sea (see Fig. 6). As data base we use the ETM+ true-colour composite LIMA, the RAMP coastline (acquired shortly before the images) was used as initialisation for the snakes. The coastline was subdivided into 703 sections for classification out of which 353 were labeled as water-to-ice, 338 as ice-to-ice and 12 as water-to-rock. Upon visual inspection we found 659 sections (94%) to be correctly classified, only 44 sections (6%) had to be manually corrected prior to further processing. The classification of adjacent regions may lead to false decisions for the type of coastline, if the initialisation is further away from the correct solution than approx. 2 km (see section 4.2). With regard to a practical application we found a manual inspection and correction of the classification results to be a reasonable solution for this problem, since checking is very fast, especially within the interactive software environment we had created for this task.
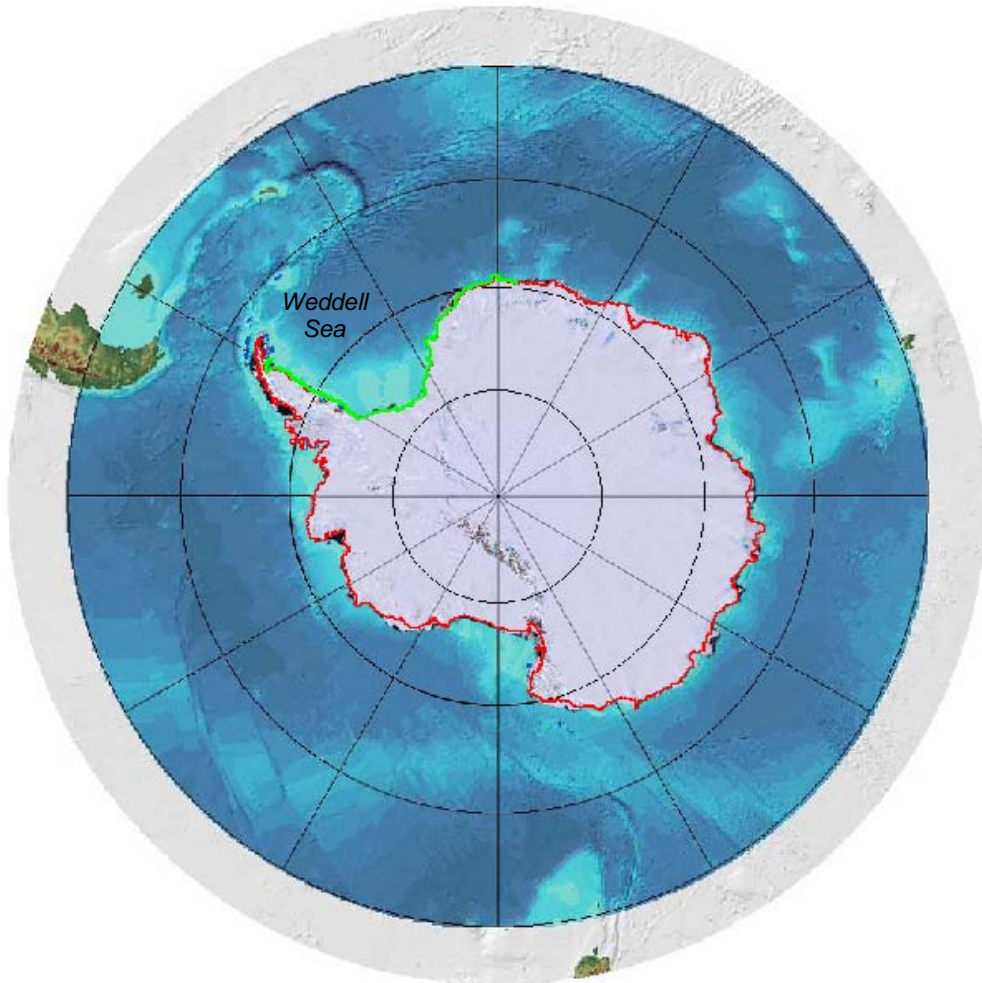
Fig. 6: Chart of the Southern Ocean sea bed topography from the General Bathymetric Chart of the Oceans (GEBCO) in the background and LIMA (centre filled with MODIS data). We have processed the green part of the coastline.

According to our model description (see chapter 3) we applied a set of default parameters for the snake optimisation. A qualitative explanation of the selected parameters is given in the following subsections. The whole list of default parameters is shown in Tab. 1.

Tab. 1: Parameter settings for the different coastline models.

| Parameter		Ice shelf to water	Ice shelf to sea ice	Rocky terrain to water
Internal Energy:	α	0.01		
	β	0.1		0.01
Image Energy:	image pre-processing	Canny edge detection	Steger line detection	HSI transformation Canny edge detection
Optimization Term:	γ	1.0		0.1
	κ	1.0		10
	max. iterations	40		

5.1 *Ice Shelf to Water*

Fig. 7 depicts a subset of LIMA that contains a coastline of the type water-to-ice. The red line marks the initial RAMP coastline. For the displayed example the initial line differs by up to 6 pixels (1.4 km) from the position indicated by the image. The high intensity contrast between the adjacent object types led to the selection of the edge model (eq. 4) as image energy. We applied the default parameters specified in Tab. 1: an intermediate value for β and a small value for κ that both lead to a relatively smooth coastline without harsh bendings still allowing the snake to manoeuvre into concave regions. The effect of an adeqate parameter β is also notable in the extraction result of (Fig. 5b) where at the tip the upper side of the initialisation is placed below the lower side of the ice shelf, and still correctly pulled towards the upper side, kept in shape by the internal energy. The optimisation term is parameterised by a large value for γ (step size) that leads to a fast convergence of the snake.
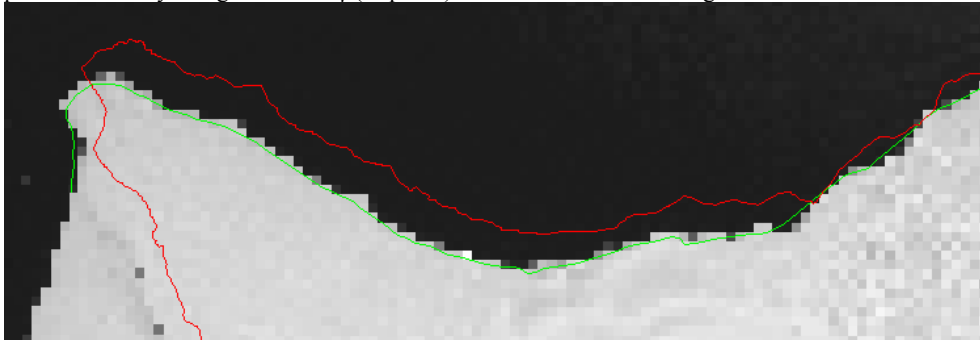
Fig. 7: Ice shelf to water model: a 28•10 km² subset of LIMA showing an ice shelf next to open water with the corresponding RAMP coastline (red) and the result of the coastline detection (green)**.**

5.2 *Ice Shelf to Sea Ice*

Fig. 8 shows a typical constellation of annual sea ice on the upper left above an ice shelf on the lower right of the green line. The initial coastline differs by up to 10 pixels (2.4 km) from the coastline in the image, visible partly as a bright line and partly as a dark line along the rift (centre part). The parameter settings for the energy terms and the snake optimisation are set similarly to those for the separation of ice and water, see section 5.1. For the image energy the line model is chosen.

(a)   (b)
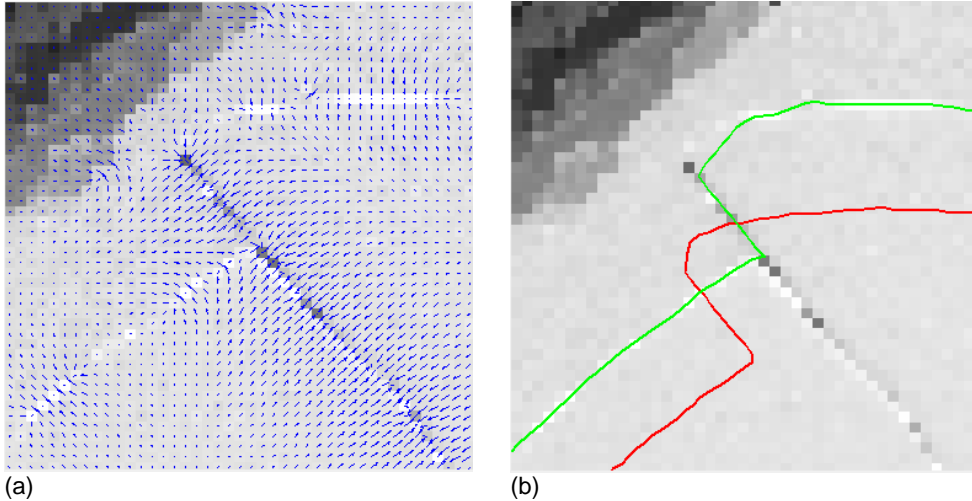
Fig. 8: Ice shelf to sea ice model: a 10•10 km² subset of LIMA showing ice shelf next to sea ice with a) the energy field based on Steger line detection; b) the corresponding RAMP coastline (red) and detection result (green). This result is identical to what we consider as ground truth.

Most of the problems that arise in this configuration are related to the lack of line-like appearance of the border line. Smaller gaps can be successfully bridged by the internal energy of the snake. Such an example can be seen in the lower left corner of Fig. 8.

5.3 *Rocky Terrain to Water*

Based on the model defined in section 3.3 the initialisation does not differ much from the coastline in LIMA. In fact, using the medium resolution image mosaic possibly downgrades the accuracy of the given coastline acquired from higher resolution data, if the coastline position has not changed over time. For the LIMA test scene (Fig. 9, top) we achieved a convergence of the snake towards the rocky coast. The coastline has moved by 1-2 pixels from the initial position, which is in fact a degration of the positional accurancy for the major parts of that coastline type. However, the result is still within the accuracy requirements for the task.

For demonstrating the payoff of the model definition we repeated this experiment with the original Landsat ETM+ image with 30 m ground resolution (see Fig. 9, bottom). Here, the initialisation (red) and detection result (green) show differences of up to 10 pixels (0.30 km), which could be removed by our method. The rocks that only show a weak contrast to the water in the intensity channel appear in a high contrast in the saturation channel, which was used in this model for defining the image energy. The saturation channel of the test area is depicted in Fig. 9 (middle), superimposed with the energy field that is oriented well towards what we consider ground trouth. We assign a small value to β and a higher weight for κ due to the potentially high curvature of the coastline.
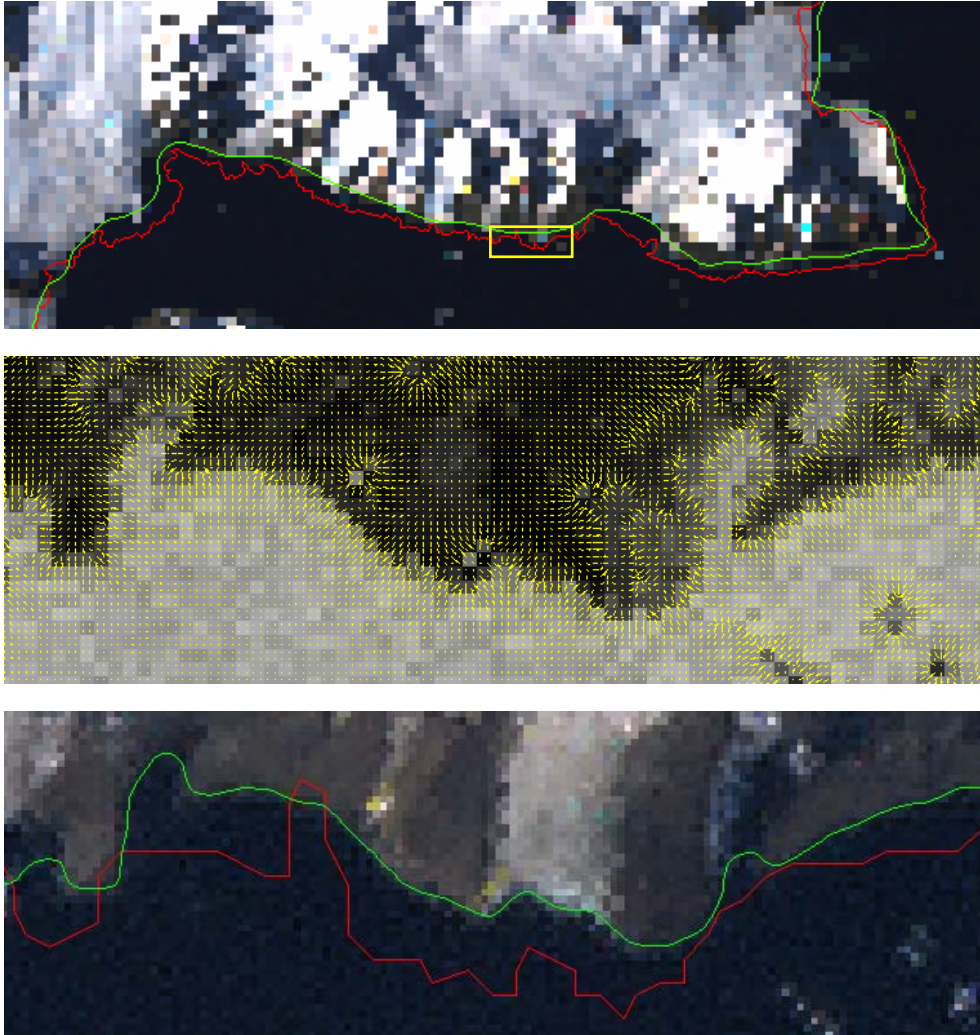
Fig. 9: Rocky terrain to water model: example shown in a 20*8 km² subset of LIMA (top); 2*0.8 km² ETM+ saturation image superimposed with the derived energy field (centre) and in RGB representation with the corresponding RAMP coastline (red) and the result of the coastline detection (green, bottom). The yellow box in the top image indicates the position of the ETM+ subset.

5.4 *Quantitative Evaluation of the Results*

For the evaluation of the proposed method, a reference dataset was extracted manually from the LIMA imagery for the coastline segment shown in Fig. 5. We then calculated the correctness (the percentage of extracted data matching the reference) and completeness (the percentage of the reference data matching the extracted data) in accordance with HEIPKE et al. (1997). With an expected geometrical accuracy for the processed coastline of 1000 m we achieved a completeness of 87.9 % and a correctness ratio of 86.3 %. In other words, 12.1 % of the manual reference cannot be detected by the approach (false negative) and 13.7 % of the obtained result is incorrect (false positives). Thus, interactive post processing is still necessary, but the human effort is significantly reduced compared

to a completely manual digitisation of the coastline. The RMS error of the true positives accounts for 380 m or approximately 1.5 pixels, which is sufficient for our purpose.

Three major issues explain the 12.1% of omitted detection. Firstly, the image energy that is selected in accordance with a local classification result may not be adequate if the initialisation lies further away from the solution than expected in the model definition due to special coastline geography like long narrow bays. Hence the snake is not assured to converge to the correct solution. Secondly, in case of ice-to-ice transition, the line response is not high along the entire scenario (see Fig. 8). This is related to the large pixel size which dampens some of the information content required for our model assumption. Thirdly, problems occur if the coastline type changes within one of the polygon segments used for classification. A scenario as in Fig. 10 requires processing with the edge model where the initial coastline (red) runs from the upper side downwards closely along the correct result in a) (green), and with the line model further down where the actual coastline is visible as a sequence of dark and bright pixels, heading towards the inbound of the ice shelf. If the sampling interval of the classification segments is too large, an inappropriate snake model might be applied within that segment leading to partially wrong solutions.

(a)   (b)
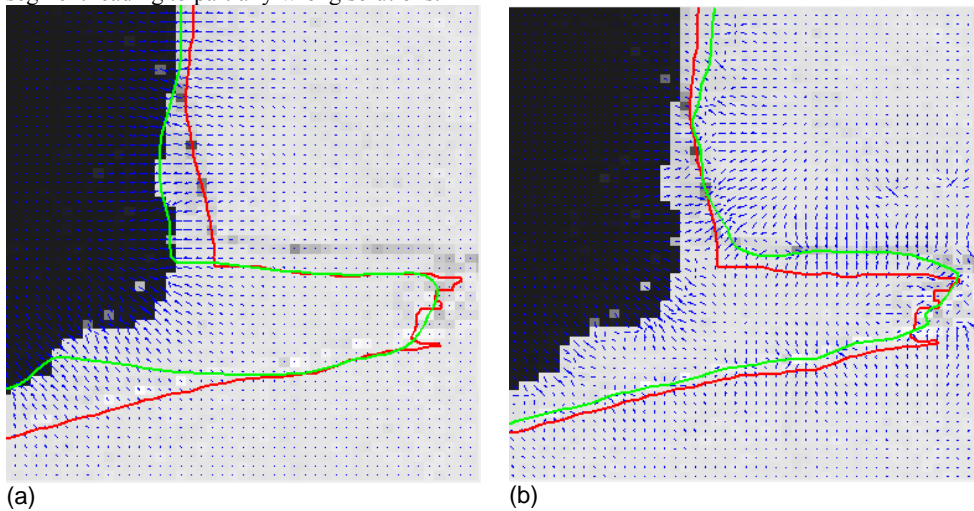
Fig. 10: Detection results using a) the edge model and b) the line model. The underlying image energy is depicted as blue vector field. The red line indicates the initialisation (identical in both cases), the green line the result. The correct choice for the final result consists of a combination of the individual results with the solution from a) for the coastal parts and from b) for the onshore.

6 Conclusions

The developed approach is capable of extracting the Antarctic coastline with a high degree of automation. Satisfying quality values can be achieved if the set of free parameters is optimised for each employed model. The proposed method of coastline extraction combines classification and updating of a given coastline in a combined scheme. The classification supports the model selection by analysing the spectral properties of the local vicinity of the coastline and significantly reduces the effort of manually assigning the correct snake model to each section of the coastline. Up to now, our classifier was based on manually selected training areas and the snake parameters were chosen empirically. We strive to incorporate more sophisticated parameter selection schemes from machine learning in future work.

In order to achieve a higher detection rate one has to further investigate the issues discussed in section 5.4. That is, on one hand, if a larger absence of image energy is encountered within the area that we consider as relevant (using an offset of 2 km in section 4.2), one could improve the classification strategy for finding the next appropriate model, e.g. by applying a stepwise increasing search radius

instead of using regions at constant distance from the initialisation. On the other hand, the impact of inappropriately chosen snake models that we experienced around transitions between different coast types, can be reduced by further decreasing the sampling intervals or by incorporating additional knowledge about land cover from other sources. Lastly, the absence of image energy encountered for the ice-to-ice model can often be circumvented by using higher resolution imagery, which already proved promising results for the rocky-terrain-to-water-model.

References

BINDSCHADLER, R., 1998: Future of the West Antarctic ice sheet. – Science **282**, p. 428.

BINDSCHADLER, R., VORNBERGER, P., FLEMING, A., FOX, A., MULLINS, J., BINNIE, D., PAULSEN, S.J., GRANNEMAN, B. & GORODETZKY, D., 2008: The Landsat Image Mosaic of Antarctica. – Remote Sensing of Environment **112**(12): 4214–4226.

BRUNT, K.M., KING, M.A., FRICKER, H.A. & MACAYEAL, D.R., 2010: Flow of the Ross Ice Shelf, Antarctica, is modulated by the ocean tide. – Journal of Glaciology **56**(195): 157–161.

BUTENUTH, M., 2008: Network Snakes. – PhD Thesis, University of Hannover, DGK-C 620.

CANNY, J., 1986: A computational approach to edge detection. – IEEE Transactions on Pattern Analysis and Machine Intelligence **8**: 679–698.

DELLA ROCCA, M.R., FIANI, M., FORTUNATO, A. & PISTILLO, P., 2004: Active Contour Model to Detect Linear Features in Satellite Images. – International Archives of Photogrammetry, Remote Sensing and Spatial Information Sciences **35**(B3): 446–450.

FUA, P., 1995: Parametric Models are Versatile: The Case of Model Based Optimization. – International Archives of Photogrammetry and Remote Sensing **XXX**(III/2): 236–246.

HEIPKE, C., MAYER, H., WIEDEMANN, C. & JAMET, O., 1997: Evaluation of automatic road extraction. – Int'l Arch. Photogrammetry Remote Sensing, **XXXII**(3-4,W2): 151–160.

HOUGHTON, J.T., DING, Y., GRIGGS, D.J., NOGUER, M., VAN DER LINDEN, P.J., DAI, X., MASKELL, K. & JOHNSON, C.A. (eds.), 2001: The Scientific Basis. Contribution of Working Group I to the Third Assessment Report of the Intergovernmental Panel on Climate Change (IPCC). – Cambridge University Press, Cambridge, United Kingdom and New York, NY, USA, 881p.

JEZEK, K. & RAMP Product Team, 2002: RAMP AMM-1 SAR Image Mosaic of Antarctica. – Fairbanks, AK: Alaska Satellite Facility, in association with the National Snow and Ice Data Center, Boulder, CO. Digital media.

KASS, M., WITKIN, A. & TERZOPOULOS, D., 1988: Snakes: Active contour models. – Int. Journal of Computer Vision **1**(4): 321–331.

LIU, H. & JEZEK, K.C., 2004: A complete high resolution coastline of Antarctica extracted from orthorectified Radarsat SAR imagery. – Photogrammetric Engineering & Remote Sensing **70**(5): 605–616.

MANDELBROT, B.B., 1967: How long is the coastline of Britain? Statistical self-similarity and fractional dimension. – Science **156**: 636–638.

MASON, D.C. & DAVENPORT, I.J., 1996: Accurate and efficient determination of shoreline in ERS-1 SAR images. – IEEE Transactions on Geoscience and Remote Sensing **34**: 1243–1253.

MUSLIM, A.M., FOODY, G.M. & ATKINSON, P.M., 2006: Localized soft classification for super resolution mapping of the shoreline. – International Journal of Remote Sensing **27**: 2271–2285.

NIEDERMEIER, A., ROMANEESSEN, E. & LEHNER, S., 2000: Detection of coastlines in SAR images using wavelet methods. – IEEE Transactions on Geoscience and Remote Sensing **38**: 2270–2281.

RYAN, T.W., SEMENTILLI, P.J., YUEN, P. & HUNT, B.R., 1991: Extraction of shoreline features by neural nets and image processing. – Photogrammetric Engineering & Remote Sensing **57**: 947–955.

SCAMBOS, T.A., HULBE, C., FAHNESTOCK, M. & BOHLANDER, J., 2000: The link between climate warming and break-up of ice shelves in the Antarctic Peninsula. – Journal of Glaciology **46**(154): 516–530.

SCAMBOS, T.A., HARAN, T.M., FAHNESTOCK, M., PAINTER, T. & BOHLANDER, J., 2007: MODIS-based Mosaic of Antarctica (MOA) datasets: Continent-wide surface morphology and snow grainsize. – Remote Sensing of Environment **111**: 242–257.

STEGER, C., 1998: An unbiased detector of curvilinear structures. – IEEE Transactions on Pattern Analysis and Machine Intelligence **20**(2): 311–326.

XU, C. & PRINCE, J.L., 1997: Gradient Vector Flow: a new external force for snakes. – IEEE Conference on Computer Vision and Pattern Recognition: 66–71.

Addresses of the authors:

Dipl.-Ing. TOBIAS KLINGER, Dipl.-Ing. MARCEL ZIEMS, Prof. Dr.-Ing. CHRISTIAN HEIPKE, Leibniz Universität Hannover, Institut für Photogrammetrie und GeoInformation, Nienburger Str. 1, D-30167 Hannover, Tel.: +49-511-762-2482, Fax: +49-511-762-2483, e-mail: <nachname>@ipi.uni-hannover.de.

Dr.-Ing. HANS WERNER SCHENKE, Dr. NORBERT OTT, Alfred-Wegener-Institut für Polar- und Meeresforschung, Van-Ronzelen-Str. 2, D-27568 Bremerhaven, Tel.: +49-471-4831-1222, Fax: +49-471-4831-1977, e-mail: hans-werner.schenke@awi.de, norbert.ott@awi.de.